The Journal of Chemical Physics

Relative energetics of CH_3CH_2O, CH_3CHOH, and CH_2CH_2OH radical products from ethanol dehydrogenation

Cite as: J. Chem. Phys. **155**, 114306 (2021); https://doi.org/10.1063/5.0062809
Submitted: 08 July 2021 . Accepted: 29 August 2021 . Published Online: 20 September 2021

Ashley E. Williams, Nathan I. Hammer, and Gregory S. Tschumper

The Journal of Chemical Physics ARTICLE scitation.org/journal/jcp

Relative energetics of CH_3CH_2O, CH_3CHOH, and CH_2CH_2OH radical products from ethanol dehydrogenation

Cite as: J. Chem. Phys. 155, 114306 (2021); doi: 10.1063/5.0062809
Submitted: 8 July 2021 • Accepted: 29 August 2021 •
Published Online: 20 September 2021

Ashley E. Williams, Nathan I. Hammer, and Gregory S. Tschumper[a)]

AFFILIATIONS

Department of Chemistry and Biochemistry, University of Mississippi, P.O. Box 1848, University, Mississippi 38677, USA

[a)]Author to whom correspondence should be addressed: tschumpr@olemiss.edu

ABSTRACT

This study has examined the relative energetics of nine stationary points associated with the three different radical isomers generated by removing a H atom from ethanol at the O atom (ethoxy, CH_3CH_2O), the α C atom (CH_3CHOH), and the β C atom (CH_2CH_2OH). For the first time, CCSD(T) geometry optimizations and harmonic vibrational frequency computations with the cc-pVTZ and aug-cc-pVTZ basis sets have been carried out to characterize two unique minima for each isomer along with three transition state structures with C_s symmetry. Explicitly correlated CCSD(T) computations were also performed to estimate the relative energetics of these nine stationary points near the complete basis set limit. These benchmark results were used to assess the performance of various density functional theory (DFT) and wave function theory methods, and they will help guide method selection for future studies of alcohols and their radicals. The structures generated by abstracting H from the α C atom have significantly lower electronic energies (by at least 7 kcal mol^{-1}) than the CH_3CH_2O and CH_2CH_2OH radicals. Although previously reported as a minimum on the ground-state surface, the $^2A''$ C_s structure of the ethoxy radical was found to be a transition state in this study with MP2, CCSD(T), and a number of DFT methods. An implicit solvation model used in conjunction with DFT and MP2 methods did not qualitatively change the relative energies of the isomers, but the results suggest that the local minima for the CH_3CHOH and CH_2CH_2OH radicals could become more energetically competitive in condensed phase environments, such as liquid water and ethanol.

I. INTRODUCTION

Oxidative degradation of ethanol in the human liver leads to production of a series of reactive oxygen species as byproducts of lipid peroxidation. These include highly reactive C_2H_5O radicals, such as the hydroxyethyl radicals (HERs), CH_3CHOH (α) and CH_2CH_2OH (b), as well as the ethoxy radical, CH_3CH_2O (O).[1–4] Oxidation of ethanol to acetaldehyde is performed by three major classes of degradative enzymes, alcohol dehydrogenases, catalases, and cytochromes. Specifically, cytochrome P450 2E1 (CYP2E1), which is present in microsomes of hepatic cells, has been implicated in the formation of the harmful HERs under study here.[5–7] Chronic ethanol exposure causes the upregulation of CYP2E1, which is responsible for the production of HERs *in vivo*, via abstraction of a hydrogen atom from ethanol.[1–4,8,9] Increased concentrations of HERs in the blood are found to correlate with liver-related injuries as well as generating autoimmune responses that attack hepatocytes. Furthermore, increased HER levels are linked to lipid peroxidation, thus being a contributor to hepatic steatosis, or "fatty liver," which occurs frequently in users exhibiting heavy alcohol use.[1,8,10]

This family of ethanol-derived radicals, denoted here as $C_2H_5O^{\bullet}$, is also of keen interest regarding their applications in the combustion of ethanol, as well as atmospheric chemistry and pollution control.[11–22] Bioethanol is a common gasoline additive. The autoignition and oxidation of ethanol occur through a variety of pathways, of which the reaction of ethanol with halogens or reaction of O + C_2H_5 and OH + C_2H_4 produces hydroxyethyl radicals as intermediates.[16,23–29] The role of hydroxyalkyl radicals in ethanol combustion has been implicated by the discovery that the enol tautomers of aldehydes are significant intermediates in ethanol combustion.[29] A number of previous studies elucidated reaction mechanisms and kinetics of the autoignition of ethanol, involving the reactions of $C_2H_5O^{\bullet}$ isomers with NO,[30] O_2,[11,20] and H_2O.[31,32]

Although CH_3CHOH is the lowest-energy isomer, the CH_2CH_2OH isomer exhibits a geometry favorable for internal abstraction, yielding the lowest dissociation pathway of the $C_2H_5O]^\bullet$ isomers to produce OH and C_2H_4 as products.[32]

Curtis *et al.* previously investigated the energies of various $C_2H_5O]^\bullet$ and $C_2H_5O]^+$ isomers.[33] They performed MP2/6-31G* geometry optimizations and G2 computations on seven conformations of the three $C_2H_5O]^\bullet$ isomers, with the lowest energy corresponding to the CH_3CHOH isomer. Two conformations of CH_3CHOH were identified. They differed only in the orientation of the hydroxyl hydrogen (*anti* vs *gauche*), with *anti*-CH_3CHOH being slightly lower in energy (0.3 kcal mol^{-1}). Additionally, they reported three stationary points of CH_2CH_2OH, again differing in the orientation of the hydroxyl hydrogen (*anti* vs *gauche*), with a second *anti*-CH_2CH_2OH minimum identified exhibiting C_s symmetry. However, these structures were reported to be ~8 kcal mol^{-1} higher in energy than the CH_3CHOH isomers. Finally, two minima were identified for the ethoxy isomer (CH_3CH_2O), one for the $^2A'$ electronic state and the other for the $^2A''$ electronic state. Both were determined to be ~10 kcal mol^{-1} higher in energy than the CH_3CHOH isomers.[33] Similar results have been obtained for the relative energetics of the CH_3CHOH, CH_2CH_2OH, and/or CH_3CH_2O isomers from other theoretical studies examining the decomposition and isomerization of $C_2H_5O]^\bullet$ with *ab initio* electronic structure methods, such as CBS-QB3, CCSD, CCSD(T), and QCISD(T).[28,32,34–38]

A total of nine $C_2H_5O]^\bullet$ structures are characterized here with full geometry optimizations and harmonic vibrational frequency computations. Given the biochemical significance of HERs, this work examines the energetics of those $C_2H_5O]^\bullet$ isomers in an aqueous environment with an implicit solvation model. CCSD(T) computations on the isolated radical species (*in vacuo*) are used to calibrate less demanding methods that are subsequently used to assess condensed phase effects on the energetics of this system.

II. THEORETICAL METHODS

Full geometry optimizations and corresponding harmonic vibrational frequency computations are performed on the C_s minimum energy structure of ethanol, CH_3CH_2OH, using density functional theory (DFT) and wave function theory (WFT) techniques, specifically the B3LYP, B3LYP-D3,[39–42] M06-2X, M06-2X-D3,[40,41,43] ω-B97XD,[44,45] ω-B97,[46] ω-B97X,[46] B2PLYP-D,[47,48] DSD-PBEP86,[49,50] PW6B95-D3,[40,41,51] M06-L, M06-L-D3,[40,41,52] MP2,[53] and CCSD(T)[54] methods. All computations for CH_3CH_2OH utilize a spin-restricted closed-shell reference function, denoted by the "r" prefix, and are performed with Dunning's correlation consistent triple-ζ basis sets with and without diffuse functions, aug-cc-pVTZ and cc-pVTZ, abbreviated here as aTZ and TZ.[55,56]

Full geometry optimizations and corresponding harmonic vibrational frequency computations are performed on the nine $C_2H_5O]^\bullet$ stationary points with the aforementioned methods and a spin-unrestricted reference function for the doublet electronic state of these radicals, denoted by the "u" prefix. All computations are performed with the aTZ and TZ basis sets. To examine potential effects from the choice of spin reference function, additional B3LYP, M06-2X, and ω-B97XD computations were performed with a spin-restricted open-shell reference function (denoted by the "ro" prefix).

A series of single point energy computations were performed on the uCCSD(T) structures optimized with the TZ and aTZ basis sets. These spin unrestricted and partially spin restricted coupled-cluster energy computations employed a high-spin restricted Hartree–Fock (RHF) reference wave function. The canonical CCSD(T) computations are denoted by RHF-uCCSD(T) and RHF-rCCSD(T), and they were carried out with the standard and augmented correlation consistent basis sets (cc-pV*X*Z and aug-cc-pV*X*Z, abbreviated here as *X*Z and a*X*Z, where *X* = D, T, Q). A suffix of either "−F12a" or "−F12b" is appended to denote the ansatz adopted for the corresponding explicitly correlated computations that employed the analogous cc-pV*X*Z-f12 basis sets, where *X* = D, T, and Q (abbreviated *X*Z-f12).[57] The spin-projected MP2 (pMP2)[58–60] energies are also reported for the corresponding uMP2 optimized structures.

To investigate the potential of solvents to affect the molecular structure and energetics, the Polarized Continuum Model (PCM)[61,62] is employed with water, ethanol, and *n*-hexane. PCM is performed exclusively with DFT and MP2 methods employing the TZ and aTZ basis sets. The Gaussian 16 software package[63] is employed for the DFT and MP2 computations. The CCSD(T) optimizations and harmonic vibrational frequency computations are performed with the CFOUR software package[64,65] using the available analytic gradients and Hessians. The canonical and explicitly correlated RHF-uCCSD(T) and RHF-rCCSD(T) single point energy computations were performed with the MOLPRO program.[66,67] These energy computations utilized the default f12 auxiliary basis sets, and the triples contributions to the CCSD(T)-F12 energies were not scaled in this investigation. The numerical integration grids, convergence criteria, and PCM solvent parameters employed herein were the default options provided for DFT methods in Gaussian 16.

III. RESULTS AND DISCUSSION

A. Optimized structures

The uCCSD(T)/TZ optimized molecular structures of the nine $C_2H_5O]^\bullet$ stationary points identified in this study are presented in Fig. 1. The uCCSD(T)/aTZ optimized structures are given in Fig. S1 of the supplementary material. Some redundant geometric parameters are reported for the C_s structures for consistency. The number of imaginary frequencies, n_i, for each structure is provided in the first row of Table I, and the corresponding uCCSD(T) harmonic vibrational frequencies can be found in the supplementary material. For comparison, the CCSD(T)/TZ and aTZ optimized structures and harmonic vibrational frequencies for ethanol, CH_3CH_2OH, are also provided in the supplementary material.

Abstraction of a hydrogen atom from ethanol at the α C (C1) produces two CH_3CHOH conformations, denoted here as *anti*-CH_3CHOH [Fig. 1(a)] and *gauche*-CH_3CHOH [Fig. 1(b)], which are predicted to be the lowest-energy structures by all of the DFT and WFT methods employed. Furthermore, the two α isomer conformations have rather similar electronic energies, with our best estimates of the CCSD(T) complete basis set (CBS) limit predicting *anti*-CH_3CHOH to be about 0.3 kcal mol^{-1} lower in energy than *gauche*-CH_3CHOH. See Sec. III B for a detailed discussion of energetics. The changes in the C1–C2 and C1–O bond lengths, ΔR,

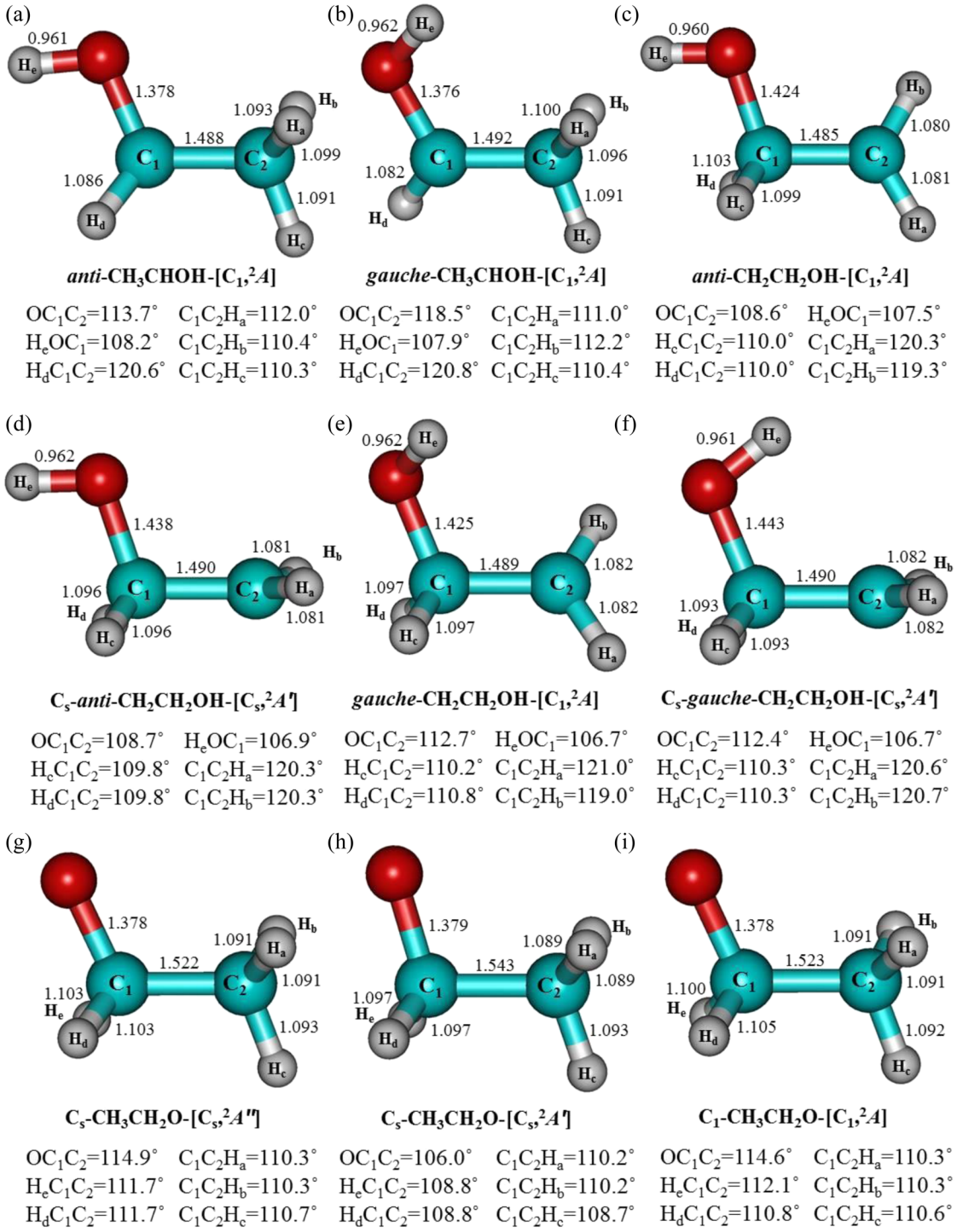

FIG. 1. uCCSD(T)/TZ optimized structures of (a) *anti*-CH_3CHOH, (b) *gauche*-CH_3CHOH, (c) *anti*-CH_2CH_2OH, (d) C_s-*anti*-CH_2CH_2OH, (e) *gauche*-CH_2CH_2OH, (f) C_s-*gauche*-CH_2CH_2OH, (g) C_s-CH_3CH_2O-$^2A''$, (h) C_s-CH_3CH_2O-$^2A'$, and (i) C_1–CH_3CH_2O-^2A. Bond lengths are presented in ångstroms and bond angles in degrees.

TABLE I. Relative electronic energies, ΔE (in kcal mol^{-1}), predicted with both canonical and explicitly correlated CCSD(T) energy computations for each CCSD(T)/TZ optimized energetic minimum. CCSD(T)/TZ optimized relative energies are included for reference.

	CH_3CHOH		CH_2CH_2OH				CH_3CH_2O		
Method	*anti* [^2A]	*gauche* [^2A]	*anti* [^2A]	C_s-*anti* [$^2A'$]	*gauche* [^2A]	C_s-*gauche* [$^2A'$]	C_s-[$^2A''$]	C_s-[$^2A'$]	C_1-[^2A]
n_i[a]	0	0	0	1	0	1	1	0	0
uCCSD(T)/TZ[b]	0	0.24	8.50	9.37	7.44	9.02	9.68	10.15	9.66
RHF-uCCSD(T)/TZ[b]	0	0.24	8.51	9.38	7.44	9.02	9.70	10.17	9.68
RHF-uCCSD(T)/QZ[b]	0	0.30	8.35	9.26	7.45	8.88	10.63	11.09	10.61
RHF-uCCSD(T)/aTZ[b]	0	0.32	8.18	9.01	7.33	8.63	10.13	10.55	10.11
RHF-uCCSD(T)/aQZ[b]	0	0.32	8.30	9.21	7.47	8.84	10.90	11.35	10.88
RHF-uCCSD(T)-F12b/DZ-f12[b]	0	0.32	8.39	9.27	7.53	8.95	10.73	11.23	10.72
RHF-uCCSD(T)-F12b/TZ-f12[b]	0	0.33	8.39	9.30	7.54	8.93	10.97	11.45	10.96
RHF-uCCSD(T)-F12b/QZ-f12[b]	0	0.33	8.39	9.32	7.55	8.94	11.10	11.59	11.09
uCCSD(T)/aTZ[c]	0	0.32	8.17	8.98	7.32	8.61	10.12	10.54	10.11
RHF-uCCSD(T)/TZ[c]	0	0.24	8.52	9.39	7.45	9.04	9.69	10.16	9.67
RHF-uCCSD(T)/QZ[c]	0	0.30	8.35	9.26	7.45	8.88	10.63	11.09	10.62
RHF-uCCSD(T)/aTZ[c]	0	0.32	8.17	8.99	7.32	8.62	10.14	10.55	10.12
RHF-uCCSD(T)/aQZ[c]	0	0.32	8.30	9.20	7.47	8.83	10.91	11.36	10.89
RHF-uCCSD(T)-F12b/DZ-f12[c]	0	0.32	8.39	9.26	7.53	8.94	10.74	11.23	10.72
RHF-uCCSD(T)-F12b/TZ-f12[c]	0	0.32	8.39	9.30	7.54	8.93	10.98	11.46	10.96
RHF-uCCSD(T)-F12b/QZ-f12[c]	0	0.32	8.39	9.32	7.55	8.94	11.11	11.60	11.10

[a]Number of imaginary vibrational frequencies from the analytic Hessians available for the uMP2, uCCSD(T), and various spin-unrestricted DFT methods with the TZ and aTZ basis sets. All frequencies are reported in the supplementary material for readers interested in the different values of n_i obtained with the default numerical integration grids and convergence criteria for certain functionals and/or basis sets.
[b]uCCSD(T)/TZ optimized geometry.
[c]uCCSD(T)/aTZ optimized geometry.

induced by dehydrogenation for the lowest-energy conformation of each isomer class are provided in Tables S4 and S5, i.e., deviations relative to ethanol. All of the DFT and WFT methods predict both the C1–C2 and C1–O bond lengths to contract by 0.031 ± 0.003 and 0.050 ± 0.004 Å, respectively, when H is removed from the α C of ethanol to form *anti*-CH_3CHOH. Interestingly, the lowest-energy $C_2H_5O]^\bullet$ isomer, *anti*-CH_3CHOH, exhibits the greatest overall geometric changes from ethanol (large contractions in both the C1–C2 and C1–O bonds).

Four CH_2CH_2OH structures [Figs. 1(c)–1(f)] were found upon abstraction of a hydrogen atom from ethanol at β C (C2), all ~8 kcal mol^{-1} higher in energy than *anti*-CH_3CHOH. All DFT and WFT computations indicate that the lowest-energy conformation of the β isomer corresponds to *gauche*-CH_2CH_2OH [Fig. 1(e)]. Our uCCSD(T) harmonic vibrational frequency computations with the TZ and aTZ basis sets show that two of the β structures characterized here correspond to transition states, C_s-*anti*-CH_2CH_2OH and C_s-*gauche*-CH_2CH_2OH, as shown in Figs. 1(d) and 1(f), respectively. Although uMP2/6-31G* frequencies indicated that the former was a minimum (n_i = 0),[33] our characterization of that stationary point is consistent with the detailed study of the CH_2CH_2OH radical by Karpichev *et al.*, indicating that this particular structure is a transition state possessing a single imaginary vibrational mode (n_i = 1) at the CCSD/6-311+G(*d*,*p*) level of theory.[34] Both C_s transition state structures of the CH_2CH_2OH radical connect equivalent forms of the corresponding minima (mirror images of *anti*- and *gauche*-CH_2CH_2OH). The electronic barrier heights associated with this conformational transition states are on the order of 1 kcal mol^{-1}. Additionally, Liu *et al.* identified a conformational transition state (TS4/4′) between the *anti*- and *gauche*-CH_2CH_2OH minima, lying ~0.6 kcal mol^{-1} above the former based on QCISD(T)/6-311G(2*df*,*p*) single point energy computations with B3LYP/6-311G(*d*,*p*) optimized structures. All of the DFT and WFT methods predict the C1–C2 bond length to contract by 0.031 ± 0.004 Å when H is removed from the β C of ethanol to form *gauche*-CH_2CH_2OH. Unlike the α isomer, the C1–O bond length in the β isomer remains practically unchanged from that of ethanol, depending on the method, at 0.000 ± 0.001 Å (Tables S4 and S5).

Finally, abstraction of the hydrogen atom from the oxygen atom in ethanol leads to the highest-energy isomer, CH_3CH_2O, with ΔE around 11 kcal mol^{-1} near the CCSD(T) CBS limit. When the CH_3CH_2O isomer has C_s symmetry, the electronic energies reported in Table I indicate that the $^2A'$ electronic state lies only ~0.5 kcal mol^{-1} above the $^2A''$ state. Although the higher-energy $^2A'$ stationary point is a minimum, the lower-energy $^2A''$ optimized structure has one imaginary frequency according to analytic Hessians computed with the uMP2, uCCSD(T), and several DFT methods using both the TZ and aTZ basis sets. Interestingly, QCISD/6-311++G(*d*,*p*) frequencies obtained by finite difference procedures did yield a single imaginary vibrational mode for the $^2A''$ C_s structure of the ethoxy radical.[28] However, B3LYP/6-311++G(*d*,*p*) frequencies computed analytically in that same study indicated that it was a minimum (n_i = 0). When the symmetry of the $^2A''$ structure is relaxed, a nearly isoenergetic C_1 minimum is identified from

subsequent uMP2, uCCSD(T), and other geometry optimizations that deviates slightly from the C_s symmetry with an O–C1–C2–H_c torsional angle near 178°. All methods consistently predict a slight elongation of the C1–C2 bond length (0.008 ± 0.002 Å) and the largest observed contraction overall in the C1–O bond length (0.056 ± 0.009 Å) when moving from ethanol to the lowest-energy O electronic state, C_1-^2A (Tables S4 and S5). This is opposite to the behavior exhibited by the β isomer, which exhibits large contractions in the C1–C2 bond length and virtually no change in the C1–O bond length.

B. Energetics

Table I provides the relative electronic energies, ΔE, for a selection of the canonical and explicitly correlated uCCSD(T) energy computations performed on the uCCSD(T)/TZ and uCCSD(T)/aTZ optimized structures. The full set of relative energies predicted by the canonical and explicitly correlated CCSD(T) energy computations is presented in the supplementary material, Tables S6 and S7. Use of an unrestricted vs restricted open-shell reference function with the DFT and MP2 methods results in virtually the same ΔE for the $C_2H_5O^{\rfloor\bullet}$ isomers. Similarly, the maximum absolute deviation (MaxAD) for ΔE between RHF-uCCSD(T) and RHF-rCCSD(T) is 0.11 kcal mol^{-1} for both canonical and explicitly correlated results. The differences between the results obtained with the a vs b ansatz for the F12 energy computations were even smaller, with a MaxAD in ΔE of 0.04 kcal mol^{-1} when employing the TZ-f12 and QZ-f12 basis sets. There is very little basis set dependence for ΔE with H abstraction from the C atoms. The canonical and F12 results are within ~0.01 kcal mol^{-1} for ΔE obtained with any quadruple-ζ basis set. ΔE for the O isomer conformations is more sensitive to the choice of basis set, as the same metric grows to ~0.5 kcal mol^{-1}.

The QZ-f12 results in Table I are near our best estimates of the CCSD(T) CBS limit and are thus used to discuss ΔE for the $C_2H_5O^{\rfloor\bullet}$ isomers, and those ΔE values do not change by more than 0.01 kcal mol^{-1} when the uCCSD(T)/aTZ optimized structures are used instead. Clearly, the *anti*-CH_3CHOH conformation of the α isomer has the lowest energy, residing 7.55 kcal mol^{-1} below *gauche*-CH_2CH_2OH and 11.10 kcal mol^{-1} below the C_1-^2A O isomer. The other conformation of the α isomer, *gauche*-CH_3CHOH, is predicted to lie only 0.33 kcal mol^{-1} higher in energy than *anti*-CH_3CHOH. The *gauche* conformation of the β isomer is confirmed to be the lowest-energy, with the *anti*-local minimum only 0.84 kcal mol^{-1} higher in energy. The QZ-f12 results in Table I indicate that ΔE is ≥11.10 kcal mol^{-1} for all O isomer structures and that the $^2A'$ minimum is only 0.50 kcal mol^{-1} above the C_1 minimum on the ground state surface of CH_3CH_2O.

A detailed analysis of the CH_2CH_2OH isomer by Karpichev *et al.* also provided relative energies near the CCSD(T) CBS limit from TZ/QZ extrapolations that are virtually identical (within 0.04 kcal mol^{-1}) to those obtained here for that subset of structures with Ref. 34. Our results presented in Table I are also consistent with published relative energetics from CCSD(T), QCISD(T), and other computations for select structures of these radical isomers,[28,32,35–38] many of which are tabulated in the supplementary material for convenience.

The RHF-uCCSD(T)-F12b/QZ-f12 relative electronic energies in Table I are employed as the reference to assess the accuracy of a series of DFT and WFT methods. Table II presents the deviations from those reference ΔE values for each optimized stationary point in kcal mol^{-1} computed with the selected methods and the TZ basis set. The average absolute deviation (AvgAD) and maximum absolute deviation (MaxAD) from the reference values are also presented. The full table of ΔE computed with the selected DFT and WFT methods and the TZ and aTZ basis sets is provided in the supplementary material, Table S6. The AvgADs and MaxADs computed with the aTZ basis set are also provided in Table S7. Although zero-point vibrational energies are not discussed here, they can be assessed from the harmonic vibrational frequencies reported in the supplementary material.

Overall, deviations from the CCSD(T) CBS limit for the DFT methods are somewhat smaller when the basis set includes diffuse functions (aTZ vs TZ); however, this trend reverses for the uMP2 and pMP2 *ab initio* methods. Based on the results in Table II, it is clear that most methods struggle to quantitatively reproduce the relative energies of the three different isomers (CH_3CHOH, CH_2CH_2OH, and CH_3H_2O). The double-hybrid functional, DSD-PBEP86, outperforms all other methods when compared to the RHF-uCCSD(T)-F12b/QZ-f12 energies with an AvgAD of 0.39 kcal mol^{-1} and MaxAD of 0.58 kcal mol^{-1}. The second double-hybrid functional B2PLYP-D also performs well compared to the other selected methods, confirming B2PLYP-D's previously described good performance in computing the energetics of small carbon-centered radicals at a reduced cost.[68] The Minnesota hybrid functional, M06-2X, and each of its variants are also among the most accurate, with uM06-2X providing an AvgAD of 0.51 kcal mol^{-1} and MaxAD of 0.91 kcal mol^{-1}. The two methods based on second-order Møller–Plesset perturbation theory provide accurate energetics when considering the CH_3CHOH and CH_2CH_2OH isomers but begin to break down when investigating the varying electronic states of the CH_3CH_2O isomer. In fact, uMP2/TZ exhibits one of the highest MaxAD's of 3.70 kcal mol^{-1}. Likewise, the pure functionals, M06-L and M06-L-D3, performed worse in computing the relative energies of the $C_2H_5O^{\rfloor\bullet}$ isomers, with an AvgAD of 2.23 kcal mol^{-1} and MaxAD of 4.51 kcal mol^{-1}.

C. Implicit solvation effects

In an effort to determine how solvation affects the energetics of the $C_2H_5O^{\rfloor\bullet}$ isomers, implicit solvation computations were performed using the Polarized Continuum Model (PCM) and three different solvents, ranging in their polarity and dielectric constants: water, ethanol, and *n*-hexane. Overall, these solvent models induced fairly small changes to the relative energies of the nine different $C_2H_5O^{\rfloor\bullet}$ structures characterized in this investigation, generally on the order of a few tenths of a kcal mol^{-1}.

The H_2O solvent model induces the largest changes to the relative energies (Table III), ranging from ~−0.4 to +0.8 kcal mol^{-1}, but the effects from ethanol are quite similar. Hexane consistently produced the smallest changes to ΔE, typically less than ±0.1 kcal mol^{-1} but reaching ~±0.2 kcal mol^{-1} for CH_3CH_2O. The values obtained with the TZ basis set tend to be slightly larger in magnitude than those computed with the aTZ basis set. The changes to ΔE for the ethanol and hexane solvent models are tabulated in the supplementary material along with the aTZ results for water.

TABLE II. Deviations (in kcal mol^{-1}) from the RHF-uCCSD(T)-F12b/QZ-f12 relative electronic energy (ΔE) values for the selected DFT and WFT methods with the TZ basis set.

	CH_3CHOH		CH_2CH_2OH				CH_3CH_2O				
Method	*anti* [^2A]	*gauche* [^2A]	*anti* [^2A]	C_s-*anti* [$^2A'$]	*gauche* [^2A]	C_s-*gauche* [$^2A'$]	C_s-[$^2A''$]	C_s-[$^2A'$]	C_1-[^2A]	AvgAD	MaxAD
uM06-L	0.00	+0.13	+1.10	+1.36	+1.16	+1.37	−4.51	−3.73	−4.49	2.23	4.51
uM06-L-D3	0.00	+0.13	+1.11	+1.37	+1.17	+1.39	−4.50	−3.71	−4.48	2.23	4.50
uB3LYP	0.00	−0.01	+1.33	+1.59	+1.10	+1.32	−2.52	−2.00	−2.51	1.55	2.52
roB3LYP	0.00	−0.01	+1.43	+1.64	+1.16	+1.42	−2.18	−1.69	−2.16	1.46	2.18
uB3LYP-D3	0.00	−0.11	+1.17	+1.47	+0.89	+1.16	−2.71	−2.31	−2.70	1.56	2.71
uM06-2X	0.00	−0.11	+0.43	+0.40	+0.18	+0.35	−0.91	−0.80	−0.90	0.51	0.91
roM06-2X	0.00	−0.11	+0.52	+0.46	+0.25	+0.48	−0.79	−0.71	−0.78	0.51	0.79
uM06-2X-D3	0.00	−0.10	+0.43	+0.40	+0.19	+0.36	−0.90	−0.78	−0.89	0.51	0.90
uωB97XD	0.00	−0.11	+1.44	+1.79	+1.28	+1.59	−2.07	−1.55	−2.05	1.49	2.07
roωB97XD	0.00	−0.11	+1.55	+1.86	+1.36	+1.73	−1.75	−1.23	−1.73	1.42	1.86
uωB97	0.00	−0.03	+1.34	+1.72	+1.28	+1.56	−2.61	−2.08	−2.60	1.65	2.61
uωB97X	0.00	−0.02	+1.37	+1.77	+1.28	+1.60	−2.34	−1.77	−2.33	1.56	2.34
uPW6B95-D3	0.00	−0.11	+1.87	+2.31	+1.62	+1.93	−2.59	−2.20	−2.58	1.90	2.59
uB2PLYP-D	0.00	−0.09	+0.85	+0.98	+0.63	+0.92	−1.15	−1.01	−1.15	0.85	1.15
uDSD-PBEP86	0.00	−0.06	+0.38	+0.43	+0.20	+0.47	−0.58	−0.44	−0.58	0.39	0.58
uMP2	0.00	−0.01	+0.14	+0.07	−0.01	+0.28	+3.70	+3.64	+3.69	1.44	3.70
pMP2	0.00	−0.02	−0.01	−0.03	−0.12	+0.09	+3.46	+3.41	+3.44	1.32	3.46
uCCSD(T)	0.00	−0.09	+0.10	+0.05	−0.11	+0.07	−1.43	−1.44	−1.43	0.59	1.44
RHF-uCCSD(T)-F12b	0.00	0.00	0.00	0.00	0.00	0.00	0.00	0.00	0.00	⋯	⋯

For the *gauche* structures of both the CH_3CHOH and CH_2CH_2OH isomers, none of the solvent models induce changes of more than ±0.1 kcal mol^{-1} at any level of theory with the TZ basis set. In contrast, the ΔE of the *anti*-conformation of CH_2CH_2OH consistently decreases by ~0.4 kcal mol^{-1} with the water and ethanol solvent models. The largest energetic effects of implicit solvation are always associated with H abstraction from the O atom, with ΔE increasing by ~0.5 to 0.7 kcal mol^{-1} when using the methods that most reliably reproduced the CCSD(T) energetics as discussed in Sec. III B (e.g., M06-2X and DSD-PBEP86).

These results can be used to estimate the relative energetics of the isomers near the CCSD(T) CBS limit in an aqueous environment

TABLE III. Shifts of the relative electronic energies (in kcal mol^{-1}) for each optimized stationary point from isolation to an implicit aqueous environment, computed with PCM and the TZ basis set.

PCM–water	CH_3CHOH		CH_2CH_2OH				CH_3CH_2O		
Method	*anti* [^2A]	*gauche* [^2A]	*anti* [^2A]	C_s-*anti* [$^2A'$]	*gauche* [^2A]	C_s-*gauche* [$^2A'$]	C_s-[$^2A''$]	C_s-[$^2A'$]	C_1-[^2A]
uM06-L	0.00	−0.10	−0.36	−0.35	+0.06	+0.02	+0.19	+0.38	+0.19
uM06-L-D3	0.00	−0.10	−0.36	−0.35	+0.06	+0.02	+0.19	+0.38	+0.19
uB3LYP	0.00	−0.09	−0.39	−0.41	+0.05	0.00	+0.32	+0.41	+0.31
uB3LYP-D3	0.00	−0.09	−0.39	−0.41	+0.02	−0.01	+0.31	+0.41	+0.31
uM06-2X	0.00	−0.08	−0.41	−0.42	+0.06	0.00	+0.55	+0.65	+0.55
uM06-2X-D3	0.00	−0.08	−0.41	−0.42	+0.06	0.00	+0.55	+0.65	+0.55
uωB97XD	0.00	−0.08	−0.37	−0.40	+0.06	+0.04	+0.43	+0.55	+0.42
uωB97	0.00	−0.07	−0.37	−0.43	+0.02	0.00	+0.48	+0.61	+0.48
uωB97X	0.00	−0.08	−0.37	−0.42	+0.04	+0.02	+0.47	+0.60	+0.47
uPW6B95-D3	0.00	−0.07	−0.38	−0.40	+0.07	+0.05	+0.35	+0.45	+0.35
uB2PLYP-D	0.00	−0.10	−0.40	−0.43	+0.01	−0.04	+0.48	+0.55	+0.48
uDSD-PBEP86	0.00	−0.09	−0.39	−0.41	+0.03	−0.03	+0.62	+0.70	+0.62
uMP2	0.00	−0.10	−0.42	−0.43	−0.01	−0.08	+0.69	+0.76	+0.69
pMP2	0.00	−0.10	−0.39	−0.44	0.00	−0.06	+0.68	+0.75	+0.68
Average	0.00	−0.09	−0.39	−0.41	+0.04	0.00	+0.45	+0.56	+0.45
Maximum	0.00	−0.10	−0.42	−0.44	+0.07	−0.08	+0.69	+0.76	+0.69
Minimum	0.00	−0.07	−0.36	−0.35	0.00	0.00	+0.19	+0.38	+0.19
Range	0.00	0.03	0.06	0.09	0.07	0.07	0.50	0.39	0.50

by combining the QZ-f12 results from Table I with the DSD-PBEP86 PCM shifts from Table III. The *anti*-conformation of CH_3CHOH still has the lowest energy of the nine structures, but the *gauche* form is only about 0.2 kcal mol^{-1} higher in energy in an aqueous environment. ΔE for the *gauche* minimum of the CH_2CH_2OH isomer remains +7.6 kcal mol^{-1}, whereas the relative energy for the *anti*-minimum decreases slightly in the water solvent model to +8.0 kcal mol^{-1} near the CCSD(T) CBS limit. The analogous estimate for the C_1 minimum of the CH_3CH_2O isomer still yields a large relative energy of +11.7 kcal mol^{-1} in an aqueous environment.

IV. CONCLUSIONS

Nine conformations of the $C_2H_5O^{\bullet}$ isomers generated by the abstraction of a hydrogen atom from ethanol at the α carbon (C1), β carbon (C2), or oxygen (O) atom have been characterized in isolation (*in vacuo*) with a range of DFT and WFT methods. Two minima have been identified for each isomer from CCSD(T) geometry optimizations and harmonic vibrational frequency computations with the TZ and aTZ basis sets, along with three transition state structures having the C_s symmetry.

RHF-uCCSD(T)-F12b/QZ-f12 computations have confirmed that the CH_3CHOH radical isomer has the lowest energy, with the *gauche* local minimum having an electronic energy roughly 0.3 kcal mol^{-1} higher than *anti*-CH_3CHOH. Four stationary points have been identified for the CH_2CH_2OH radical isomer. The *gauche*-CH_2CH_2OH structure has the lowest electronic energy of these four conformations, all of which lie at least 7.5 kcal mol^{-1} higher than *anti*-CH_3CHOH according to CCSD(T) electronic energies near the CBS limit. Three CH_3CH_2O isomer structures have been reported, each with $\Delta E \geq +11$ kcal mol^{-1} according to our RHF-uCCSD(T)-F12b/QZ-f12 single point energy computations. The $^2A''$ C_s structure of the CH_3CH_2O radical was found to be a transition state with the MP2, CCSD(T), and most DFT methods, which led to the identification of a C_1 minimum on the doublet ground state surface that deviates only slightly from the $^2A''$ transition state structure.

Analysis of the accuracy of a selection of DFT and WFT methods has revealed that M06-2X and the double-hybrid functionals (uB2PLYP-D and uDSD-PBEP86) outperform the other DFT and WFT methods employed here in reliably computing relative energetics of the $C_2H_5O^{\bullet}$ isomers when compared to the benchmark ΔE values. The effects of solvation on the energetics and molecular geometries of the $C_2H_5O^{\bullet}$ isomers have also been investigated with PCM computations employing the default solvent parameters for water, ethanol, and hexane. Although no large, qualitative changes were observed in the $C_2H_5O^{\bullet}$ energetics when moving from isolation to an implicit solvent model, the local minima of the CH_3CHOH and CH_2CH_2OH isomers became more energetically competitive in water and ethanol. A subsequent study is planned to investigate this effect in greater detail by explicitly solvating these radical isomers with water and ethanol molecules to form a diverse set of clusters spanning a wide range of sizes and hydrogen bonding topologies.

SUPPLEMENTARY MATERIAL

The relative energies obtained with the DFT methods mentioned above and the TZ and aTZ basis sets can be found in the supplementary material along with the harmonic vibrational frequencies computed with all levels of theory. The deviations in energies and geometries induced by implicit solvation models in ethanol and hexane are presented to support our conclusion. The Cartesian coordinates for the nine $C_2H_5O^{\bullet}$ structures examined in this study are also provided.

AUTHORS' CONTRIBUTIONS

All authors contributed equally to this work.

ACKNOWLEDGMENTS

This work was supported, in part, by the National Science Foundation (Grant No. CHE-1664998). The Mississippi Center for Supercomputing Research (MCSR) is also acknowledged for allocation of time on their computational resources.

The authors have no conflicts to disclose.

DATA AVAILABILITY

Data from the geometry optimizations and corresponding harmonic vibrational frequency computations for each $C_2H_5O^{\bullet}$ isomer conformation are available from the corresponding author upon reasonable request.

REFERENCES

[1] E. Albano, S. W. French, and M. Ingelman-Sundberg, Front. Biosci. **4**, D533–D540 (1999).
[2] E. Albano, P. Clot, M. Morimoto, A. Tomasi, M. Ingelman-Sundberg, and S. W. French, Hepatology **23**, 155–163 (1996).
[3] E. Albano, A. Tomasi, L. Goria-Gatti, and M. U. Dianzani, Chem.-Biol. Interact. **65**, 223–234 (1988).
[4] L. A. Reinke, Y. Kotake, P. B. McCay, and E. G. Janzen, Free Radical Biol. Med. **11**, 31–39 (1991).
[5] A. Dey and S. M. Kumar, Cell Biol. Toxicol. **27**, 285 (2011).
[6] N. A. Osna and T. M. Donohue, Jr., Subcell. Biochem. **67**, 177–197 (2013).
[7] S. Zakhari, Alcohol Res. Health **29**, 245–254 (2006).
[8] M. I. Díaz Gómez, G. D. Castro, A. M. A. Delgado de Layo, M. H. Costantini, and J. A. Castro, Toxicology **154**, 113–122 (2000).
[9] D. R. Moore, L. A. Reinke, and P. B. McCay, Mol. Pharmacol. **47**, 1224–1230 (1995).
[10] C. P. Day and O. F. W. James, Gastroenterology **114**, 842–845 (1998).
[11] G. da Silva, J. W. Bozzelli, L. Liang, and J. T. Farrell, J. Phys. Chem. A **113**, 8923–8933 (2009).
[12] E. E. Dames, Int. J. Chem. Kinet. **46**, 176–188 (2014).
[13] H. Feng, J. Zhang, X. Wang, and T. H. Lee, Fuel **234**, 836–849 (2018).
[14] H. Hashemi, J. M. Christensen, and P. Glarborg, Fuel **218**, 247–257 (2018).
[15] C. J. Hayes, D. R. Burgess, and J. A. Manion, "Combustion pathways of biofuel model compounds: A review of recent research and current challenges pertaining to first-, second-, and third-generation biofuels," in *Advances in Physical Organic Chemistry*, edited by I. H. Williams and N. H. Williams (Academic Press, 2015), Chap. 3, pp. 103–187.
[16] B. Karpichev, L. W. Edwards, J. Wei, and H. Reisler, J. Phys. Chem. A **112**, 412–418 (2008).
[17] K. Kohse-Höinghaus, P. Oßwald, T. A. Cool, T. Kasper, N. Hansen, F. Qi, C. K. Westbrook, and P. R. Westmoreland, Angew. Chem., Int. Ed. **49**, 3572–3597 (2010).
[18] A. Millán-Merino, E. Fernández-Tarrazo, M. Sánchez-Sanz, and F. A. Williams, Combust. Flame **215**, 221–223 (2020).

[19]S. M. Sarathy, P. Oßwald, N. Hansen, and K. Kohse-Höinghaus, Prog. Energy Combust. Sci. **44**, 40–102 (2014).
[20]J. Zádor, R. X. Fernandes, Y. Georgievskii, G. Meloni, C. A. Taatjes, and J. A. Miller, Proc. Combust. Inst. **32**, 271–277 (2009).
[21]J. Zádor, C. A. Taatjes, and R. X. Fernandes, Prog. Energy Combust. Sci. **37**, 371–421 (2011).
[22]X. Wang, J. Song, and Z. Meng, J. Phys. Chem. A **123**, 7544–7549 (2019).
[23]C. Anastasi, V. Simpson, J. Munk, and P. Pagsberg, J. Phys. Chem. **94**, 6327–6331 (1990).
[24]P. A. Cleary, M. T. B. Romero, M. A. Blitz, D. E. Heard, M. J. Pilling, P. W. Seakins, and L. Wang, Phys. Chem. Chem. Phys. **8**, 5633–5642 (2006).
[25]K. Hoyermann, M. Olzmann, J. Seeba, and B. Viskolcz, J. Phys. Chem. A **103**, 5692–5698 (1999).
[26]S. Rudić, C. Murray, D. Ascenzi, H. Anderson, J. N. Harvey, and A. J. Orr-Ewing, J. Chem. Phys. **117**, 5692–5706 (2002).
[27]B. Ruscic and J. Berkowitz, J. Chem. Phys. **101**, 10936–10946 (1994).
[28]J. P. Senosiain, S. J. Klippenstein, and J. A. Miller, J. Phys. Chem. A **110**, 6960–6970 (2006).
[29]C. A. Taatjes, N. Hansen, A. McIlroy, J. A. Miller, J. P. Senosiain, S. J. Klippenstein, F. Qi, L. Sheng, Y. Zhang, T. A. Cool, J. Wang, P. R. Westmoreland, M. E. Law, T. Kasper, and K. Kohse-Höinghaus, Science **308**, 1887–1889 (2005).
[30]Y. Liu, X. Li, G. Tian, X. Li, and Z. Sun, Comput. Theor. Chem. **1032**, 84–89 (2014).
[31]T. Zhang, M. Wen, Y. Ju, J. Kang, R. Wang, J. Cao, and S. K. Roy, J. Phys. Org. Chem. **32**, e3895 (2019).
[32]E. Kamarchik, L. Koziol, H. Reisler, J. M. Bowman, and A. I. Krylov, J. Phys. Chem. Lett. **1**, 3058–3065 (2010).
[33]L. A. Curtiss, D. J. Lucas, and J. A. Pople, J. Chem. Phys. **102**, 3292–3300 (1995).
[34]B. Karpichev, L. Koziol, K. Diri, H. Reisler, and A. I. Krylov, J. Chem. Phys. **132**, 114308 (2010).
[35]G.-X. Liu, Y.-H. Ding, Z.-S. Li, Q. Fu, X.-R. Huang, C.-C. Sun, and A.-C. Tang, Phys. Chem. Chem. Phys. **4**, 1021–1027 (2002).
[36]Z. F. Xu, K. Xu, and M. C. Lin, ChemPhysChem **10**, 972–982 (2009).
[37]R. S. Zhu, J. Park, and M. C. Lin, Chem. Phys. Lett. **408**, 25–30 (2005).
[38]B. L. J. Poad, A. W. Ray, and R. E. Continetti, J. Phys. Chem. A **117**, 12035–12041 (2013).
[39]A. D. Becke, J. Chem. Phys. **98**, 5648–5652 (1993).
[40]S. Grimme, J. Antony, S. Ehrlich, and H. Krieg, J. Chem. Phys. **132**, 154104 (2010).
[41]S. Grimme, S. Ehrlich, and L. Goerigk, J. Comput. Chem. **32**, 1456–1465 (2011).
[42]C. Lee, W. Yang, and R. G. Parr, Phys. Rev. B **37**, 785–789 (1988).
[43]Y. Zhao and D. G. Truhlar, Theor. Chem. Acc. **120**, 215–241 (2008).
[44]D. A. Boese, ChemPhysChem **16**, 978–985 (2015).
[45]J.-D. Chai and M. Head-Gordon, Phys. Chem. Chem. Phys. **10**, 6615–6620 (2008).
[46]J.-D. Chai and M. Head-Gordon, J. Chem. Phys. **128**, 084106 (2008).
[47]S. Grimme, J. Chem. Phys. **124**, 034108 (2006).
[48]T. Schwabe and S. Grimme, Phys. Chem. Chem. Phys. **9**, 3397–3406 (2007).
[49]S. Kozuch and J. M. L. Martin, Phys. Chem. Chem. Phys. **13**, 20104–20107 (2011).
[50]S. Kozuch and J. M. L. Martin, J. Comput. Chem. **34**, 2327–2344 (2013).
[51]Y. Zhao and D. G. Truhlar, J. Phys. Chem. A **109**, 5656–5667 (2005).
[52]Y. Zhao and D. G. Truhlar, J. Chem. Phys. **125**, 194101 (2006).
[53]C. Møller and M. S. Plesset, Phys. Rev. **46**, 618–622 (1934).
[54]G. D. Purvis III and R. J. Bartlett, J. Chem. Phys. **76**, 1910–1918 (1982).
[55]R. A. Kendall, T. H. Dunning, Jr., and R. J. Harrison, J. Chem. Phys. **96**, 6796–6806 (1992).
[56]D. E. Woon and T. H. Dunning, Jr., J. Chem. Phys. **98**, 1358–1371 (1993).
[57]K. A. Peterson, D. E. Woon, and T. H. Dunning, Jr., J. Chem. Phys. **100**, 7410–7415 (1994).
[58]P. J. Knowles, Chem. Phys. Lett. **155**, 513–517 (1989).
[59]P. J. Knowles and N. C. Handy, J. Chem. Phys. **88**, 6991–6998 (1988).
[60]C. Sosa and H. B. Schlegel, Int. J. Quantum Chem. **32**, 267–282 (1987).
[61]R. Cammi and J. Tomasi, J. Comput. Chem. **16**, 1449–1458 (1995).
[62]S. Miertuš, E. Scrocco, and J. Tomasi, Chem. Phys. **55**, 117–129 (1981).
[63]M. J. Frisch, G. W. Trucks, H. B. Schlegel, G. E. Scuseria, M. A. Robb, J. R. Cheeseman, G. Scalmani, V. Barone, G. A. Petersson, H. Nakatsuji, X. Li, M. Caricato, A. V. Marenich, J. Bloino, B. G. Janesko, R. Gomperts, B. Mennucci, H. P. Hratchian, J. V. Ortiz, A. F. Izmaylov, J. L. Sonnenberg, D.Williams-Young, F. Ding, F. Lipparini, F. Egidi, J. Goings, B. Peng, A. Petrone, T. Henderson, D. Ranasinghe, V. G. Zakrzewski, J. Gao, N. Rega, G. Zheng, W. Liang, M. Hada, M. Ehara, K. Toyota, R. Fukuda, J. Hasegawa, M. Ishida, T. Nakajima, Y. Honda, O. Kitao, H. Nakai, T. Vreven, K. Throssell, J. A. Montgomery, Jr., J. E. Peralta, F. Ogliaro, M. J. Bearpark, J. J. Heyd, E. N. Brothers, K. N. Kudin, V. N. Staroverov, T. A. Keith, R. Kobayashi, J. Normand, K. Raghavachari, A. P. Rendell, J. C. Burant, S. S. Iyengar, J. Tomasi, M. Cossi, J. M. Millam, M. Klene, C. Adamo, R. Cammi, J. W. Ochterski, R. L. Martin, K. Morokuma, O. Farkas, J. B. Foresman, and D. J. Fox, Gaussian 16 Rev. B.01, Wallingford, CT, 2016.
[64]J. G. J. F. Stanton, M. E. Harding, P. G. Szalay, CFOUR, coupled-cluster techniques for computational chemistry, with contributions from A. A. Auer, R. J. Bartlett, U. Benedikt, C. Berger, D. E. Bernholdt, Y. J. Bomble, L. Cheng, O. Christiansen, M. Heckert, O. Heun, C. Huber, T.-C. Jagau, D. Jonsson, J. Jusélius, K. Klein, W. J. Lauderdale, D. A. Matthews, T. Metzroth, L. A. Mück, D. P. O'Neill, D. R. Price, E. Prochnow, K. Ruud, F. Schiffmann, W. Schwalbach, S. Stopkowicz, A. Tajti, J. Vázquez, F. Wang, J. D. Watts and the integral packages MOLECULE (J. Almlöf and P. R. Taylor), PROPS (P. R. Taylor), ABACUS (T. Helgaker, H. J. Aa. Jensen, P. Jørgensen, and J. Olsen), and ECP routines by A. V. Mitin and C. van Wüllen, available at http://www.cfour.de.
[65]D. A. Matthews, L. Cheng, M. E. Harding, F. Lipparini, S. Stopkowicz, T.-C. Jagau, P. G. Szalay, J. Gauss, and J. F. Stanton, J. Chem. Phys. **152**, 214108 (2020).
[66]H. J. Werner, P. J. Knowles, R. D. Amos, A. Bernhardsson, A. Berning, P. Celani, D. L. Cooper, M. J. O. Deegan, A. J. Doobbyn, F. Eckert, C. Hampel, G. Hetzer, T. Korona, R. Lindh, A. W. Lloyd, S. J. McNicholas, F. R. Manby, W. Meyer, M. E. Mura, A. Nicklass, P. Palmieri, R. Pitzer, G. Rauhut, M. Schutz, U. Schumann, H. Stroll, A. J. Stone, R. Tarroni, and T. Thorsteinsson, MOLPRO version 2019.2, a package of *ab initio* programs, 2019.
[67]H.-J. Werner, P. J. Knowles, G. Knizia, F. R. Manby, and M. Schütz, Wiley Interdiscip. Rev.: Comput. Mol. Sci. **2**, 242–253 (2012).
[68]P. R. Tentscher and J. S. Arey, J. Chem. Theory Comput. **8**, 2165–2179 (2012).